CHIN. PHYS. LETT. Vol. 29, No. 6 (2012) 068101

Green Emission from a Strain-Modulated InGaN Active Layer *

WANG Guo-Biao(王国彪)[1], XIONG Huan(熊欢)[1], LIN You-Xi(林友熙)[1], FANG Zhi-Lai(方志来)[1**], KANG Jun-Yong(康俊勇)[1], DUAN Yu(段雨)[2], SHEN Wen-Zhong(沈文忠)[2]

[1]*Semiconductor Photonics Research Center, Department of Physics, Xiamen University, Xiamen 361005*
[2]*Key Laboratory of Artificial Structures and Quantum Control (Ministry of Education), Department of Physics, Shanghai Jiao Tong University, Shanghai 200240*

(Received 9 January 2012)

Strain-induced quantum dots (QDs) like island formations are demonstrated to effectively suppress pits/dislocation generation in high indium content (26.8%) InGaN active layers. In addition to the strain redistribution in the QD-like islands, strain modulation on the InGaN active layers by using the GaN island capping is employed to form an increased surface potential barrier around the dislocation cores, which inhibits the carrier transport to the surrounding dislocations. Cathodoluminescence shows distinct double-peak emissions at 503 nm and 444 nm, corresponding to the In-rich QD-like emission and the normal quantum well emission, respectively. The QD-like emission becomes dominated in photoluminescence due to the carrier localization effect of In-rich InGaN QDs at relatively low "carrier injection current". Accordingly, green emission may be enhanced by the following origins: (1) reduction in pits/dislocations density, (2) carrier localization and strain reduction in QDs, (3) strain modulation by GaN island capping, (4) enhanced light extraction with faceted GaN islands on the surface.

PACS: 81.07.−b, 81.05.Ea, 78.67.−n, 68.65.−k DOI: 10.1088/0256-307X/29/6/068101

As a newly emerging lighting technology, semiconductor-based solid state lighting has made remarkable progress in the past decade and may replace conventional incandescent and fluorescent technologies in the next decade.[1−4] One of the limitations for InGaN-based general lighting applications is the significant drop in internal quantum efficiency (IQE) for the InGaN-based green light emitting diodes (LEDs).[5−7] With the increase of indium content in InGaN, the alloy phenomena and formation of threading dislocations (TDs)/stacking faults related surface pits would become severe, resulting in poor crystalline quality for the green InGaN/GaN quantum wells (QWs).[5,6] Moreover, strong strain-induced piezoelectric polarization fields (PFs) would further reduce the overlapping of electron-hole wave functions, and thus significantly reduce the IQE of the InGaN-based green LEDs.[6,7]

Various methods have been employed to improve the crystalline qualities as well as to overcome the negative effects of PFs on the IQE of the InGaN-based materials and devices by use of lattice matched AlGaInN barriers, Si-doped GaN barriers, InGaN triangular QWs or nonpolar/semipolar growth.[8−13] An alternative method is to reduce the piezoelectric PFs along the polar direction by strain redistribution/reduction via quantum dot (QD) formation, which has been regarded as a promising technique for fabrication of high-brightness green light sources.[14,15] In this work, strain-induced island growth is employed to form high-density InGaN QDs. The surface pit density is significantly reduced by strain-induced island formation, which suppresses the nonradiative recombination at the pits/TDs sites. On the InGaN QDs, GaN islands are subsequently grown as the top barrier. Interestingly, the GaN islands preferentially nucleate near the TDs leading to strain-modulated relatively high surface potential barrier surrounding the TDs, which causes lateral carrier confinement away from nonradiative recombination at the defects and thus enhances the light emission efficiency.

The metalorganic vapor phase epitaxy (MOVPE) of GaN films and InGaN/GaN QWs was carried out on c-sapphire substrates. Trimethylgallium, trimethylindium, and high-purity ammonia were used as the source precursors and silane as the n-type dopant. Firstly the sapphire substrates were cleaned at 1060℃ and 100 Torr for 15 min in H_2 ambient followed by nitridation at 550℃ for 4 min. A conventional GaN nucleation layer was grown at 535℃ and 500 Torr followed by a high-temperature annealing process. The subsequent growth of a ∼1.6-μm-thick GaN epilayer was carried out at 1035℃ and 100 Torr. For the sample Q1, bare InGaN layers grown by MOVPE at 670℃ for 90 s (nominal thickness of ∼3.3 nm) on the surface modified GaN templates, which has been demonstrated to improve the growth of InGaN/GaN QWs and also enhance the QW emission.[16] Relatively thin InGaN layers were grown for the avoidance of significant strain generation and

*Supported by the National Natural Science Foundation of China under Grant Nos 60876008 and 61076091, and the Program for New Century Excellent Talents in Fujian Province University.
**To whom correspondence should be addressed. Email: zhilaifang@hotmail.com

the consequent plastic strain relaxation via pits/TDs formation. Growth of InGaN layers at relatively low temperature reduced the adatom diffusion and thus favored the island growth mode. Before temperature ramping for the growth of high-temperature barrier layers, an ultrathin low-temperature GaN layer was grown at the well temperature for suppressing the indium outdiffusion to the barrier layers.[17] Further growth of GaN cap on the InGaN/GaN QWs was carried out for the sample Q2. A moderate ramp rate (about 1 K/s) for the temperature ramping process from the growth temperature of InGaN QW to that of GaN barriers was employed for continuous and gradual relaxation of the thermal strain, which may prevent a considerable increase of thermal strain and thus suppress the consequent pits/TDs formation. Further, without long annealing under H_2 ambient, significant morphology changes of the InGaN layers caused by the annealing effect may be avoided.[18] In order to clarify the annealing effect, sample Q1A was grown with the same processes like that for the sample Q1, but with an additional "annealing" process (ramping from 670℃ to 786℃ in 108 s) followed by a fast cooling process.

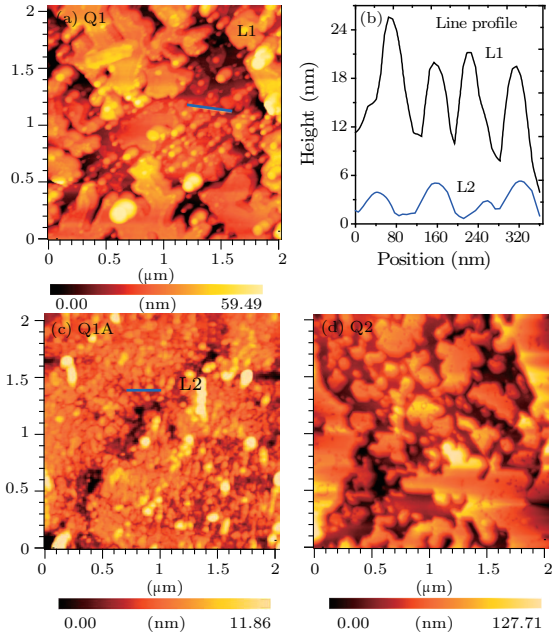

Fig. 1. (a) The surface morphology of the sample Q1. (b) Typical line profiles over the islands of the samples Q1 and Q1A. The surface morphology of the samples (c) Q1A and (d) Q2.

The surface morphology of the InGaN epilayers and InGaN/GaN QWs was investigated by atomic force microscopy (AFM). The microstructure of the InGaN/GaN QWs was investigated by high-resolution transmission electron microscopy (TEM). The spatially-resolved luminescence was measured by a scanning electron microscope (SEM) combined with cathodoluminescence (CL) at room temperature (RT). The surface chemical compositions were analyzed by x-ray photoelectron spectroscopy (XPS). The RT photoluminescence (PL) excited by a 325 nm He-Cd laser was measured for the InGaN epilayers and the InGaN/GaN QWs.

Figure 1(a) shows a typical surface morphology of the bare InGaN layers for the sample Q1. The surface is island-like with an rms surface roughness of 10.8 nm and island density of about $4.0 \times 10^9\,\mathrm{cm}^{-2}$. An island line profile L1 is drawn in Fig. 1(b). The average island size and height are about 60 nm and 10 nm, respectively. Generally, for strain relaxation there is an interplay/coexistence between plastic relaxation (for significant strain) via misfit dislocation generation and elastic strain relaxation via coherent island formation (for strain below a critical value).[19] Relatively thin InGaN layers were grown for the avoidance of significant strain generation and the consequent plastic strain relaxation via pits/TDs formation. Growth of InGaN layers at relatively low temperature reduced the adatom diffusion and thus favored the island growth mode. Therefore, for the sample Q1, strain-induced island formation becomes possible, leading to the island-like surface feature. As a result, the overall strain of the relatively thin QW layer can be partially released by the island formation, which suppresses the pits/TDs generation.

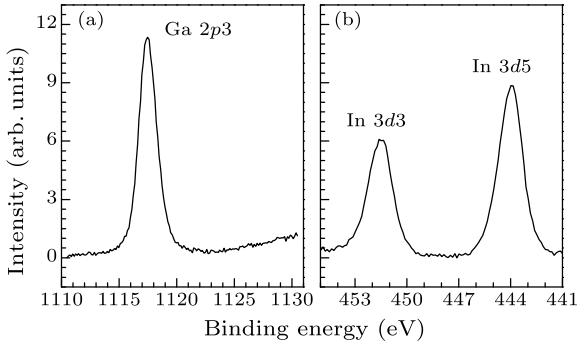

Fig. 2. XPS spectra of the (a) Ga 2*p*3 and (b) In 3*d* photoelectron peaks of the sample Q1.

On the InGaN layers a high-temperature GaN barrier was subsequently grown. It has been reported that the temperature ramp for the barrier growth may alter the morphology of the InGaN layer to a interlinking network of InGaN strips if annealing for a relatively long time (240–960 s) under H_2 ambient.[18] Both the prolonged annealing and the introduction of H_2 would enhance the InGaN decomposition.[20] Accordingly, in this study, relatively fast ramping (108 s) and lack of H_2 introduction were employed for the avoidance of obvious morphology changes of the InGaN layers. As shown in Fig. 1(c) for the surface morphology of the sample Q1A, the QD-like surface structure is still evident as that of the sample Q1, indicating that the QD-like islands formed during the growth of the InGaN

layers would not be significantly influenced by the temperature ramping process employed in this study. An island line profile L2 is drawn in Fig. 1(b). The island size and height are about 65 nm and 4.5 nm, respectively. After temperature ramps, a small increase in island lateral size and a small decrease in island height can be observed, suggesting the tendency of adatom diffusion from the island top to the bottom, or relatively fast decomposition rate for the top island materials. After temperature ramping from 670℃ to 786℃, GaN cap was subsequently grown on the InGaN QD-like islands. As shown in Fig. 1(d) for the sample Q2, the island size increases whereas the island density decreases to about $1.2 \times 10^9\,\mathrm{cm}^{-2}$. The presence of InGaN QD-like islands on the surface increases the nucleation sites for the subsequent growth of the GaN cap, leading to preferential nucleation of GaN at the edges of the InGaN QD-like islands. After island coarsening and coalescence, the small InGaN QD-like islands were buried in the large GaN islands.

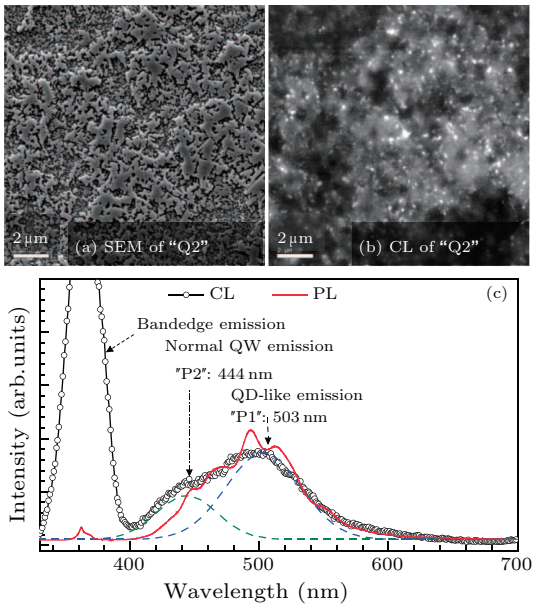

Fig. 3. (a) SEM and (b) RT CL images, and (c) RT PL and CL spectra of the sample Q2.

XPS was employed for further compositional analysis of the InGaN layers. Figure 2(a) shows the XPS spectrum (after background subtraction and intensity normalization to the Ga 2p3 peak) of the Ga 2p3 photoelectron peak for the samples T1 and Q1, whereas Fig. 2(b) shows that of the In 3d peak. The percentage of indium composition can be estimated by

$$X_{\mathrm{In}} = \frac{I_{\mathrm{In}3d5}/F_{\mathrm{In}3d5}}{I_{\mathrm{In}3d5}/F_{In3d5} + I_{\mathrm{Ga}2p3}/F_{\mathrm{Ga}2p3}},$$

where I denotes the integrated intensity of the XPS photoelectron peaks and F the sensitivity factors ($F_{\mathrm{Ga}2p3} = 2.75$ and $F_{\mathrm{In}3d5} = 4.53$). The indium content is roughly estimated to be as high as ∼26.8% for the sample Q1, due to the enhanced indium incorporation at relatively low growth temperature and formation of high-density In-rich InGaN QDs on the surface.

Figure 3 shows the spatially-resolved luminescence properties of the sample Q2 investigated by SEM-CL at room temperature. As shown in Fig. 3(a), discrete islands distributed over the surface were observed. Correspondingly, in the CL image of Fig. 3(b) distinct bright spots were observed at the island sites, indicating the presence of strong exciton localization correlated with the InGaN QDs buried in the GaN islands; very weak emission was observed at the non-island sites. It is expected that a number of QDs would be embedded in one GaN island. Further, the emission intensity of different QD-like islands varied in a wide range due to the variations in island size, height, and composition. Therefore, it is reasonable that the observed bright spot density (∼$3.0\times10^8\,\mathrm{cm}^{-2}$) in the CL image is less than the QD-like island density observed in the AFM image. Figure 3(c) shows the RT CL and PL spectra of the sample Q2. In addition to the GaN bandedge emission at 365 nm, distinct double-peak CL emission from the InGaN active layers (black dotted line) was observed at 503 nm corresponding to the In-rich QD-like emission (see the cyan dash line, fitted peak P1) and at 444 nm corresponding to the normal QW emission (see green dashed line, fitted peak P2), respectively. The emission peak broadening is likely caused by variations in indium content and shape of the QD-like islands. RT PL (red line curve) has also been employed to investigate the luminescence properties. Apparently, the QD-like emission dominates indicating the carrier localization effect of QDs at relatively low carrier injection current in PL compared with that in CL. At high carrier injection current for CL measurements, carriers may escape from the In localized states (In-rich QDs) and recombine in QWs leading to the increased QW emission in CL.

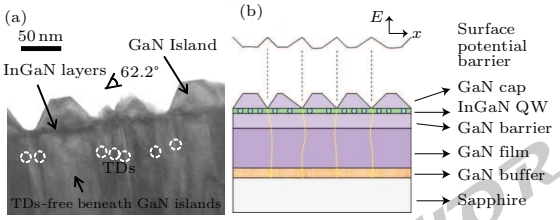

Fig. 4. (a) The cross-sectional TEM image of the sample Q2. (b) Schematic diagram of the epitaxial structure and the surface potential energy barrier fluctuation caused by the strain modulation of the GaN islands on the InGaN active layers for the sample Q2.

Figure 4(a) shows the cross-sectional TEM image of the sample Q2. The epitaxial structure is drafted in Fig. 4(b). The variation of dark contrast in the InGaN QWs is likely correlated with the presence of strained In-rich InGaN QDs. Faceted GaN islands

of the $\{1\bar{1}01\}$ sidewall faceting were observed on the surface with an island size of about 50–200 nm and a sidewall polar angle of 62.2°. As discussed previously, preferential nucleation of GaN at the edges of the InGaN QD-like islands results in GaN island formation around the InGaN QD-like islands. Further, taking into account the reduced Ga incorporation rate on the $\{1\bar{1}01\}$ planes and at the TDs sites, GaN islanding with the $\{1\bar{1}01\}$ sidewall faceting around the QDs on the TDs-free sites is preferred. This is followed by GaN island coarsening, coalescence and terminating at the TDs sites with a reduced GaN barrier height around the TDs cores (circled), as observed by TEM. Considering the geometry of the strain modulation effect on the InGaN active layers induced by the GaN islands, relatively high surface potential barriers around the TDs sites are formed, as illustrated in Fig. 4(b), showing the surface potential barrier fluctuation at different sites. Such an increasing potential barrier around the TDs cores causes the lateral carrier confinement away from nonradiative recombination at the defects and thus enhances the light emission efficiency. Further, formation of faceted GaN islands on the emission surface may increase the light extraction efficiency.

In conclusion, by strain-induced QD-like island formation, misfit dislocation/pit generation is suppressed during the growth of thin InGaN layers at low temperature. Continuous and gradual thermal strain relaxation by a moderate temperature ramping for GaN barrier growth prevents a considerable increase of thermal strain and thus suppresses the consequent pit/TD formation. Relatively short "annealing" time without introduction of H_2 is employed to suppress the InGaN decomposition phenomena. Spatially resolved SEM-CL shows high density bright spots at the island sites whereas very weak emission from the non-island sites, indicating the presence of carrier localization effect correlated with the InGaN QDs buried in the GaN islands. RT CL shows distinct double-peak emissions at 503 nm and 444 nm, corresponding to the In-rich QD-like emission and the normal QW emission, respectively. RT PL of relatively low "carrier injection current" shows dominated QD-like emission, which further supports the carrier localization effect of In-rich InGaN QDs. TEM microstructure analysis exhibits faceted GaN islands on the InGaN active layers with TDs locating between neighboring islands and a reduced barrier height around the TDs cores. Accordingly, strain modulation on the InGaN active layers caused by the GaN islands on top resulted in a relatively high surface potential barrier around the TDs cores. We hereby summarize the origins for the enhanced green emission as: (1) reduction in pits/TDs density decreases the nonradiative recombination rate, (2) strain redistribution via QD formation enhances the overlapping of electron-hole wave functions, (3) both carrier localization in QDs and the increased surface potential barrier around the TDs cores inhibit the transport of carriers to the surrounding dislocations and defects and their eventual nonradiative recombination, and (4) enhancement in light extraction efficiency by surface roughening.

References

[1] Schubert E F and Kim J K 2005 *Science* **308** 1274
[2] Schubert E F, Kim J K, Luo H and Xi J Q 2006 *Rep. Prog. Phys.* **69** 3069
[3] Humphreys C J 2008 *MRS Bull.* **33** 459
[4] Fang Z L 2011 *Nanotechnology* **22** 315706
[5] Lin Y S, Ma K J, Hsu C, Feng S W, Cheng Y C, Liao C C, Yang C C, Chou C C, Lee C M and Chyi J I 2000 *Appl. Phys. Lett.* **77** 2988
[6] Li T, Fischer A M, Wei Q Y, Ponce F A, Detchprohm T and Wetzel C 2010 *Appl. Phys. Lett.* **96** 031906
[7] Feneberg M and Thonke K 2007 *J. Phys.: Condens. Matter* **19** 403201
[8] Schubert M F, Xu J, Kim J K, Schubert E F, Kim M H, Yoon S, Lee S M, Sone C, Sakong T and Park Y 2008 *Appl. Phys. Lett.* **93** 041102
[9] Park E H, Kang D N H, Ferguson I T, Park S K and Yoo T K 2007 *Appl. Phys. Lett.* **90** 031102
[10] Zhao H P, Arif R A and Tansu N 2009 *IEEE J. Sel. Top. Quantum Electron.* **15** 1104
[11] Lin Y X and Fang Z L 2011 *Appl. Phys.* A **103** 317
[12] Feezell D F, Schmidt M C, Denbaars S P and Nakamura S 2009 *MRS Bull.* **34** 318
[13] Fang Z L, Lin Y X and Kang J Y 2011 *Appl. Phys. Lett.* **98** 061911
[14] Schulz S and O'Reilly E P 2010 *Phys. Rev.* B **82** 033411
[15] Arakawa Y 2002 *IEEE J. Sel. Top. Quantum Electron.* **8** 823
[16] Fang Z L, Kang J Y and Shen W Z 2009 *Nanotechnology* **20** 045401
[17] Fang Z L, Lin D Q, Kang J Y, Kong J F and Shen W Z 2009 *Nanotechnology* **20** 235401
[18] Oliver R A, Sumner J, Kappers M J and Humphreys C J 2009 *J. Appl. Phys.* **106** 054309
[19] Tersoff J and LeGoues F K 1994 *Phys. Rev. Lett.* **72** 3570
[20] Koleske D D, Wickenden A E, Henry R L, Culbertson J C and Twigg M E 2001 *J. Cryst. Growth* **223** 466